(2)

NRL Memorandum Report 5366

AD-A144 432

# Theory of Vorticity Generation by Shock Wave and Flame Interactions

J. M. PICONE, E. S. ORAN, J. P. BORIS, AND T. R. YOUNG, JR.

*Laboratory for Computational Physics*

July 5, 1984

DTIC FILE COPY

This work was supported by the Office of Naval Research.




NAVAL RESEARCH LABORATORY
Washington, D.C.

## REPORT DOCUMENTATION PAGE

| | |
|---|---|
| 1a REPORT SECURITY CLASSIFICATION<br>UNCLASSIFIED | 1b RESTRICTIVE MARKINGS |
| 2a SECURITY CLASSIFICATION AUTHORITY | 3 DISTRIBUTION/AVAILABILITY OF REPORT<br>Approved for public release; distribution unlimited. |
| 2b DECLASSIFICATION DOWNGRADING SCHEDULE | |
| 4 PERFORMING ORGANIZATION REPORT NUMBER(S)<br>NRL Memorandum Report 5366 | 5 MONITORING ORGANIZATION REPORT NUMBER(S) |
| 6a NAME OF PERFORMING ORGANIZATION<br>Naval Research Laboratory<br>6b OFFICE SYMBOL (If applicable)<br>Code 4040 | 7a NAME OF MONITORING ORGANIZATION |
| 6c ADDRESS (City, State, and ZIP Code)<br>Washington, DC 20375 | 7b ADDRESS (City, State, and ZIP Code) |
| 8a NAME OF FUNDING/SPONSORING ORGANIZATION<br>Office of Naval Research<br>8b OFFICE SYMBOL (If applicable) | 9 PROCUREMENT INSTRUMENT IDENTIFICATION NUMBER |
| 8c ADDRESS (City, State, and ZIP Code)<br>Arlington, VA 22217 | 10 SOURCE OF FUNDING NOS<br>PROGRAM ELEMENT NO: 61153N; PROJECT NO: RR011-09-43; TASK NO: ; WORK UNIT NO: DN280-071 |
| 11 TITLE (Include Security Classification)<br>(See page ii) | |
| 12 PERSONAL AUTHOR(S)<br>Picone, J.M., Oran, E.S., Boris, J.P., and Young, T.R., Jr. | |
| 13a TYPE OF REPORT<br>Interim<br>13b TIME COVERED FROM TO | 14 DATE OF REPORT (Yr, Mo, Day)<br>July 5, 1984<br>15 PAGE COUNT<br>32 |
| 16 SUPPLEMENTARY NOTATION<br>This work was supported by the Office of Naval Research. | |
| 17 COSATI CODES<br>FIELD / GROUP / SUB GR | 18 SUBJECT TERMS (Continue on reverse if necessary and identify by block number)<br>Combustion<br>Turbulence |

19 ABSTRACT (Continue on reverse if necessary and identify by block number)

We present detailed numerical and theoretical studies of vorticity generation by the interaction of a weak planar shock with an azimuthally symmetric flame. The calculations are two-dimensional and correspond to a cylindrical flame. To analyze the fluid-dynamic aspects of the problem, we exclude chemical reactions and model the flame as a region of reduced density and elevated temperature. We find that the rotational flows associated with the vorticity distribution are long-lived and can produce a significant distortion of the heated region. The results of our numerical simulations and the estimates of the nonlinear theory are quite consistent. We also compare the nonreactive numerical simulations with the experimental data of Markstein on shock wave and flame interactions in a stoichiometric mixture of n-butane and air. The numerical simulations reproduce most of the major experimental observations. We show that conventional Rayleigh-Taylor instability theory, which assumes a very small initial perturbation, does not provide a viable description of vorticity generation in Markstein's experiment. Instead, a nonlinear treatment based on the finite misalignment and finite interaction time of the pressure gradient associated with the shock and the density gradient

(Continues)

| | |
|---|---|
| 20 DISTRIBUTION/AVAILABILITY OF ABSTRACT<br>UNCLASSIFIED/UNLIMITED ☒ SAME AS RPT ☐ DTIC USERS ☐ | 21 ABSTRACT SECURITY CLASSIFICATION<br>UNCLASSIFIED |
| 22a NAME OF RESPONSIBLE INDIVIDUAL<br>J.M. Picone | 22b TELEPHONE NUMBER (Include Area Code)<br>(202) 767-6326<br>22c OFFICE SYMBOL<br>Code 4040 |

DD FORM 1473, 83 APR EDITION OF 1 JAN 73 IS OBSOLETE

11. TITLE (Include Security Classification)

Theory of Vorticity Generation by Shock Wave and Flame Interactions

19. ABSTRACT (Continued)

of the flame is necessary. The effects of chemical reactions are also clarified through the comparison of numerical simulation and experiment.

CONTENTS

# THEORY OF VORTICITY GENERATION BY SHOCK WAVE AND FLAME INTERACTIONS

## INTRODUCTION

The interaction of pressure waves with density gradients is a fundamental source of long-lived vorticity in fluids (Chu and Kovásznay, 1957, and Picone and Boris, 1983). This mechanism is particularly important in combustion, since the release of chemical energy produces both pressure and density disturbances in the fluid. These disturbances then interact, producing significant vorticity. The rotational motion associated with the vorticity field enhances mixing and introduces additional fluctuations in the flow variables. The scale lengths which characterize these secondary fluctuations are roughly one-half those of the local density gradients which exist prior to interacting with given pressure waves (Picone and Boris, 1983). Because the structures and sizes of the fluid interfaces change under the influence of the newly generated vorticity, local reaction rates change, amplifying the effects of the fluctuations and producing more local pressure waves. The process thus continues, progressively reducing the length scales of inhomogeneities in the flow field. Through this mechanism, a flow which is originally laminar can quickly become turbulent. Such phenomena occur in almost every nonidealized high Reynolds number flow.

In this paper, we focus on the interaction of a weak, planar shock wave with an azimuthally symmetric region characterized by density and temperature distributions similar to those found in an expanding flame. Our calculations are two-dimensional and correspond to a cylindrical flame. This problem contains the essential features of vorticity generation by pressure wave and flame interactions. Ignoring the flame dynamics is acceptable for calculating the large-scale vorticity distribution, since the transit time of the shock

Manuscript approved February 1, 1984.

across the heated region is quite short compared to the time scale of flame propagation. Markstein has studied a similar case experimentally for a reactive medium, using a long, vertical shock tube with a 30 cm combustion chamber at the bottom and a diaphragm 90 cm from the top. Figure 1 shows Schlieren photographs from one of Markstein's experiments. A weak shock (pressure ratio ~ 1.3) passes through a roughly spherical flame approximately 15 cm from the bottom of the chamber, which contains a stoichiometric mixture of n-butane and air. In the first frame, we see the incident shock less than 1 cm from the flame boundary. The flame actually appears to be more oblong than spherical. In the second photograph, for which time is defined to be 0.10 ms, we see a curved rarefaction wave moving upward from the flame while the upper flame boundary has been compressed by the flow behind the incident shock. By 0.40 ms, a vortex ring has formed due to the interaction of the shock wave and the flame. The enhanced flow at the center of the ring pulls unreacted gas through the flame, causing the gas to ignite. As the newly ignited gas emerges, a fine-grained turbulent burning zone develops (apparent at 0.70 ms).

To analyze the fluid-dynamic aspects of vorticity generation, we will study the closely related situation in which a planar shock interacts with a hot, low density region in a nonreactive fluid. Past treatments of this problem have relied on the linearization of all or part of the relevant equations or have used a perturbation expansion (Rudinger, 1958, and Markstein, 1964). Those approaches are valid for cases with vanishingly small perturbation amplitudes and time scales but cannot provide a quantitative picture of the large scale flows which result from the initial asymmetries, for which the characteristic length scale is the flame radius and the interaction time scale is finite.

In the next section, we outline a simple nonlinear theory of vorticity generation by shock wave and flame interactions. We then present the results of a two-dimensional numerical simulation of the nonreactive case. The simulation provides a clear picture of the formation of a vortex ring. The calculation also provides a calibration of constants arising in the theory. Finally, we discuss the shock wave and flame interaction as a mechanism for developing and enhancing turbulence and for determining the set of turbulent scales observed experimentally.

## NONLINEAR THEORY

Equation (1) gives the rigorous, inviscid equation for the time evolution of vorticity,

$$\frac{d\underset{\sim}{\xi}}{dt} + \underset{\sim}{\xi}\,\underset{\sim}{\nabla}\cdot\underset{\sim}{v} = \underset{\sim}{\xi}\cdot\underset{\sim}{\nabla}\,\underset{\sim}{v} + \left(\underset{\sim}{\nabla}\rho \times \underset{\sim}{\nabla}P\right)/\rho^2, \qquad (1)$$

where $\underset{\sim}{v}$ is the fluid velocity, $\underset{\sim}{\xi} = \underset{\sim}{\nabla} \times \underset{\sim}{v}$ is the vorticity, $\rho$ is the density, and P is the pressure. All variables are functions of the position $\underset{\sim}{r}$ and time t. Equation (1) provides a direct mechanism for the generation of vorticity by shock wave and flame interactions, since the right hand side contains a source term which is proportional to the cross product of the density and pressure gradients. Whenever the local pressure and density gradients are misaligned, the source term will be nonzero and the production of vorticity will occur. In Fig. 1, the experimental case of interest, the pressure gradient associated with the planar shock is parallel to the axis of the shock tube while the density gradient of the spherical flame is directed approximately radially outward from the center. Large scale vorticity in the form of a vortex ring results from the interaction.

An estimate of vorticity generation in the nonreactive case by this mechanism requires the integration of Eq. (1) in both space and time. We may, however, simplify our task by working in two dimensions (Cartesian), since the induced rotational flows, which are cylindrically symmetric, differ from those of a vortex ring by geometrical factors of order one (see sentence

following Eq. (5) below). We then exploit the fact that after the shock has passed through a circular region of density variation in the x-y plane, the residual flow field consists of a pair of vortices of strength $\pm \kappa_z \equiv \pm \kappa$ (Picone and Boris, 1983). Figure 2 defines the notation for this section and the Appendix. For the purpose of integrating Eq. (1) analytically, we align the x-axis with the direction of propagation of the shock and place the origin at the center of the density depression. The quantity $S_0$ denotes the radius of the heated region, and the vortices will be centered at $(x,y) \approx (0, \pm \bar{y})$, where $\bar{y} \lesssim S_0$. That is, in the case of a planar shock propagating downward through a circular heated region in a two-dimensional vertical chamber, there will be one vortex on either side of the vertical axis of the chamber. The pair of vorticies will be roughly centered on the heated region, and the associated rotational flows will be oppositely directed. The strength of one vortex at time t is equal to the integral of the vorticity over the half plane containing the vortex. For the case of interest, the vortex strength is

$$\kappa_z(t) = \int_0^\infty dy \int_{-\infty}^{\infty} dx \; \xi_z(x,y,t), \tag{2}$$

which satisfies the equation (see the Appendix)

$$\frac{d\kappa_z}{dt} \approx \int_0^\infty dy \int_{-\infty}^{\infty} dx \; [(\nabla\rho \times \nabla P)_z / \rho^2]. \tag{3}$$

In a formal sense, the residual vortex strength is then

$$\kappa \equiv \lim_{t \to \infty} \kappa_z(t). \tag{4}$$

In practice, the generation of vorticity occurs over a finite time interval $(-\tau/2, \tau/2)$. For an azimuthally symmetric density depresssion with a characteristic radius $S_0$, the time interval $\tau$ is approximately equal to $2S_0/W$, where W is the average velocity with which the shock propagates across the region. Because this time is much shorter than the time required for the resulting rotational flows to affect the density gradient appreciably, we may ignore the feedback effects of the vorticity on the generation process.

Given the value of $\kappa$, we may compute the fluid velocity along the line bisecting the vortex pair by summing the flows induced by each vortex separately. Because the azimuthal velocity of an isolated vortex filament has the magnitude $|v_\theta| = |\kappa|/2\pi r$, where r is the radial distance from the center of the filament, we obtain

$$v_x(x,0) \approx |\kappa|\ \bar{y}/\pi(x^2 + \bar{y}^2). \tag{5}$$

Notice that the maxiumum value is $|\kappa|/\pi\bar{y}$, which agrees closely with $|\kappa|/2\bar{y}$, the corresponding velocity for a vortex ring. We may define the mixing time scale $\tau_{mix}$ as the interval over which a fluid element travels from $(-S_0, 0)$ to $(S_0,0)$ under the influence of the residual flows. Integrating Eq. (5) gives

$$\tau_{mix} = 2\pi S_0(S_0^2/3 + \bar{y}^2)/|\kappa|\bar{y}\ . \tag{6}$$

In Fig. 1, we notice that the compression of the hot region by the flows behind the shock has reduced the distance that the fluid elements must travel to reach the lower edge of the heated region. Thus our $\tau_{mix}$ will be larger than the actual transit time.

In the Appendix, we compute the integral in Eq. (4) for the case of a planar shock passing through a cylindrically symmetric density depression like that in Fig. 1. We find that, prior to the return of the reflected shock from the end of the shock tube,

$$\kappa \approx 2\, v_2(1 - v_2/2W)\, S_0\, \ell n(\rho_\infty/\rho_0)\, f$$
$$\approx 2\, v_2(W - v_2/2)\, (\tau/2)\, \ell n(\rho_\infty/\rho_0)\, f, \qquad (7)$$

where $f \lesssim 1$ is a form factor which varies with the initial density profile. In Eq. (7), $v_2$ is the flow velocity behind the shock in the laboratory frame; W is the shock velocity; $\rho_\infty$ is the ambient density of the unburned medium; and $\rho_0$ is the density at the center of the spherical flame. For a shock of pressure ratio 1.3 and $\gamma = 1.4$, the Rankine-Hugoniot relations give us $v_2 \approx W/6$ and $W \approx 1.12\, c_s$, where $c_s$ is the ambient sound speed prior to passage of the shock. In our simulation $S_0 \approx 2.5$ cm, $\rho_\infty/\rho_0 \approx 9.5$, and $c_s \approx 3.4 \times 10^4$ cm/s. Equation (7) gives us a vorticity strength of $\kappa \lesssim 6 \times 10^4 \text{cm}^2/\text{s}$. For $\bar{y} \lesssim S_0$, the time scale $\tau_{mix}$ for a fluid element to be pulled from one side of the heated region to the other ($\Delta x = 2S_0$) under the influence of the residual vorticity is $\lesssim 900\,\mu$s. This is consistent with the simulation results (Fig. 5) and with Markstein's experiment (Fig. 1), which shows that fluid is pulled through the center of the burning zone prior to the arrival of the reflected shock approximately 600 $\mu$s after the vorticity is generated. We note again that in the spherical case the fluid velocity through the center of the vortex ring is 50% higher than that for the two-dimensional model which we have used here. Thus the shorter time scale ($\tau_{mix}$) of Markstein's experiment is consistent with the estimate given above. Because the region of density variation is no longer azimuthally symmetric, the reflected shock should increase the number of vortex centers.

## NUMERICAL SIMULATION

We have used the two-dimensional reactive shock model (Oran et al., 1983), which is based on the code FAST2D (Book et al., 1981), to simulate the interaction between a weak planar shock and a cylindrically symmetric density depression in air. The algorithm employs time-step splitting in conjunction with flux-corrected transport (FCT) (Boris and Book, 1976) to solve the equations for conservation of mass, momentum, and energy. The reactive shock model also contains algorithms for chemical kinetics, energy release, and thermal and molecular diffusion. We have calibrated the code extensively through studies of shocks on wedges in nonreactive fluids (Book et al., 1981) and studies of detonation cell structure, which required models of energy release (Oran et al., 1983). In the present simulations, we used Cartesian geometry and did not include chemical reactions or diffusive transport processes.

The Cartesian grid consisted of 150 x 50 cells of dimension 0.2 cm on each side. The grid remained fixed throughout the calculation. Thus the simulated chamber was 30 cm x 10 cm, as in Markstein's experiment. We have aligned the x-axis with the axis of the shock tube. The simulation had inflow boundary conditions with $\underset{\sim}{v} = (v_2, 0)$ at the side from which the shock propagated, where $v_2$ is the velocity behind the shock in the laboratory frame. The other boundaries were reflecting. A typical timestep was $\Delta t_s \approx 1 \mu s$, where the subscript $s$ indicates simulated time. Figure 3 is a density contour diagram approximately 90 μs (simulated time) after the simulation began. The density contours run from $3.0 \times 10^{-4}$ to $1.26 \times 10^{-3}$ g/cm$^3$ in equal increments.

Figure 4 shows the initial density and temperature profiles more clearly. The density profile had the convenient functional form

$$\rho(r) = \rho_\infty + (\rho_0 - \rho_\infty)/[1+(r/S_0)^2]^2 \quad . \tag{8}$$

The shock pressure ratio was 1.3, again similar to Markstein's experiment (Rudinger, 1958, and Markstein, 1964), and the shock moved from top to bottom. The ambient pressure was 1.0 atm, and the ratio of principal specific heats $\gamma(\equiv c_p/c_v)$ was constant at the value 1.4. The ambient density ($\rho_\infty$) and temperature ($T_\infty$) were $1.17 \times 10^{-3}$ g/cm$^3$ and 300K, respectively, while the minimum density ($\rho_0$) and peak temperature ($T_0$) were $1.24 \times 10^{-4}$ g/cm$^3$ and 2840K. To compare simulation times ($t_s$) with those in Markstein's experiment, one should subtract approximately 150μs from the simulated time.

Figures 5-7 show the evolution of the density, pressure, and vorticity, respectively. The x-axis is vertical to facilitate comparisons with Fig. 1; thus the shock initially propagates downward in the figures. There are striking similarities to the experimental photographs (Fig. 1). Figure 4 shows that the density distribution is compressed by the shock and the entire heated region is pulled toward the bottom of the chamber by the flows behind the shock. The reflected rarefaction wave and curved transmitted shock are clearly visible in Fig. 6. The curvature of the latter occurs because of the increased sound speed inside the heated region. An interesting feature is the Mach structure caused by reflection of the curved shock by the chamber. The sequence of density diagrams clearly demonstrates the effects of the vortex pair, which has pulled ambient gas from the top of the heated region to the bottom in a time $\tau_{mix} \lesssim 1$ ms, consistent with both Fig. 1 and our theory. The

vorticity contours in Fig. 7 show the existence of two long-lived vortices which are equal in magnitude and oppositely directed. Sometime after the shock has passed through the heated region ($t_s \sim 500\mu s$), the simulation gives a vortex strength $\kappa \sim 3 \times 10^4$ cm$^2$/s, which is consistent with the theoretical estimate.

Another point of considerable interest is the enhancement of the vorticity by subsequent shocks. The vorticity has a maximum magnitude of approximately $1.1 \times 10^4$ s$^{-1}$ just before the reflected shock strikes the heated region ($t_s = 722\mu s$), and $1.8 \times 10^4$ s$^{-1}$ afterward ($t_s = 1.4$ ms). Note the reduction in size and the increased number of the vortex centers between those times in Fig. 7, indicating the role of successive pressure waves in the evolution of a structure more like that found in turbulent flows.

Because the release of chemical energy was not included in the calculation and because of the resolution limitations of the calculation, several noteworthy differences exist between the experiment and the simulation. First we notice in the density contour diagrams that the heated region spreads and that the innermost contour disappears by $t_s = 600\mu s$, indicating that cooling occurs as the ambient gas is pulled through the center by the vortices. In a reactive medium, the ambient gas would ignite, at least maintaining the temperature and producing pressure waves, which would hasten the transition to turbulence. The reactions would also alter the reflected shock. Figure 1 ($t = 0.70$ ms) shows that the reflected shock wave actually emerges as a dark band above the vortex ring. Finally, the limited resolution of the calculation and the omission of three-dimensional effects have prevented much of the cascade to small scale turbulence, which appears in Fig. 1. Despite these limitations, the simulation has revealed major fluid-dynamic effects in shock wave and flame interactions.

## COMPARISON WITH RAYLEIGH-TAYLOR INSTABILITY THEORY

Previous analyses of shock wave and flame interactions have used or have suggested using a modified version of conventional Rayleigh-Taylor instability theory (see, for example, Rudinger, 1958, and Markstein, 1964). Indeed, Markstein (private communication) has pointed out that such an analysis, with proper choices of parameters, gives a result similar to Eq. (7). In the usual Rayleigh-Taylor picture, the length scale of the initial perturbation is infinitesimal or "small", while the source term in Eq. (1),

$$\underset{\sim}{S} = \underset{\sim}{\nabla}\rho \times \underset{\sim}{\nabla}P/\rho^2 \tag{9}$$

is nonzero for a "long" period of time compared to the growth rate of the perturbation. Markstein (1964) modified this to account for the short time scale of the shock passage through a perturbed (rippled) flame boundary. He demonstrated the phenomenon experimentally by passing a smooth flame through a wire grid to perturb the flame boundary prior to the arrival of a planar shock. As expected, the small ripples in the flame surface were amplified by the perturbed flow field caused by the shock. These features were, however, soon overwhelmed by nonlinear effects. Because the unperturbed flame was hemispherical, the passage of the planar shock produced large scale vorticity, which obliterated the smaller features.

In this paper, we have been concerned with the more general, nonlinear description of vorticity generation. Thus we are addressing situations in which the length scale of the perturbation is finite (flame radius) and the source term is also nonzero over the time period during which the shock passes through the entire flame. Because both scales are finite, we require a

nonlinear integration of Eq. (1), which covers the entire spectrum of inviscid vorticity-generating phenomena. We note that, even for perturbations of small spatial and temporal extent, the analysis of the flow field over long time periods must include nonlinear effects.

## SUMMARY

We have presented both an analytic theory and numerical simulations of the vorticity generated by a planar shock wave passing through a hot region similar to that of a flame. In order to extract the basic fluid-dynamic mechanism in this interaction, we have restricted our work to two dimensions and have excluded chemical reactions. This is a good approximation for the calculation of the large scale vorticity distribution, since the laminar flame moves much slower than the shock. Our analysis has shown that, after the shock passes through the flame, a residual rotational flow field remains. This flow field is equivalent to that of a vortex pair (or a vortex ring in three dimensions) characterized by a circulation $\kappa$ (Eq. 7). The separation $\bar{y}$ of the filaments is $\lesssim S_0$, the radius of the heated region. We have also defined and computed a mixing time scale for the vorticity distribution which is consistent with Markstein's experiment (Fig. 1) and the simulations.

Our numerical simulations of a planar shock interacting with a cylindrically symmetric region of reduced density used our reactive shock model, which is based on the FAST2D computer code. The computer model was identical to that used previously to study detonation structure (Oran et al., 1983); only the boundary and initial conditions were different. From the simulations, we have determined the time development of the flow field as well as the flows which remain after the shock has passed through the flame. The simulations agree well with experiment and theory, and show that conventional

Rayleigh-Taylor instability theory does not provide an adequate description of vorticity generation. The source of large scale vorticity for the case studied here is the initial large-scale misalignment of pressure and density gradients present in the fluid.

The general framework presented in this paper applies to vorticity generation by any pressure perturbation interacting with a density gradient. Examples of this phenomenon include sound waves or shocks passing through flames, hot spots, or boundary layers; the key ingredient is the misalignment of the pressure and density gradients as the interaction occurs. We conclude that pressure waves produced in one portion of a reacting medium will generate or enhance turbulence as the waves encounter density fluctuations within the medium. The scale lengths of the additional turbulence will be less than the spatial size of the original density fluctuations. We have thus described and demonstrated a mechanism for producing turbulence in reactive systems and have developed a framework for calculating the strength and the scales on which the turbulence is generated.

## ACKNOWLEDGMENTS

The authors gratefully acknowledge support for this work by the Office of Naval Research. We also acknowledge support by the Defense Advanced Research Projects Agency (DARPA Order No. 4395) which funded the initial theoretical and numerical investigations leading to the work reported here. The comments of Mr. John Gardner, Dr. Raafat Guirguis, and Dr. K. Kailasanath have been most helpful. In addition, we thank Dr. George Markstein of Factory Mutual Research Corporation for his comments and his kind assistance in obtaining a print of Fig. 1.

## APPENDIX - PLANAR SHOCK INTERACTION

We will analyze the case shown in Fig. 2 by considering (in two dimensions) a planar shock interacting with a circular heated region. The symbol W denotes the velocity of the shock through the burning zone. and $\rho_2$, $v_2$, and $P_2$ are the density, fluid velocity. and pressure behind the shock. The corresponding quantities ahe d of the shock are $\rho_1$, $v_1(\sim 0)$, and $P_1$. The hot gas has a radius $S_0$, and the time $t \equiv 0$ occurs when the shock reaches the center of the burning zone. Here we will assume that the shock is weak (pressure ratio $P_2/P_1 \approx 1.3$) and that the pressure and density ratios do not change significantly when the shock enters the burning zone. The circular shape of the hot flame and the elevated speed of sound in the interior of the flame cause the shock to become curved upon passing through the heated region. Our analysis will not account for this curvature. We represent the flow field of the shock as follows:

$$\begin{bmatrix} \rho \\ P \\ v \end{bmatrix} \equiv \begin{bmatrix} \rho_1 \\ P_1 \\ v_1 \end{bmatrix} + \begin{bmatrix} \rho_2 - \rho_1 \\ P_2 - P_1 \\ v_2 - v_1 \end{bmatrix} f_\alpha(s, \theta, W, t) \quad , \tag{A1}$$

where s and 0 define the position of a point relative to the center of the heated region, $\alpha$ is a parameter defining shock thickness, $f_\alpha$ satisfies the relation

$$\lim_{\alpha \to 0} f_\alpha \equiv \begin{cases} 1 - h(\cos\theta) & , t = 0 \\ h(s \cos\theta/Wt - 1) & , t < 0 \\ 1 - h(s \cos\theta/Wt - 1) & , t > 0, \end{cases} \tag{A2}$$

and h(u) is the unit step function,

$$h(u) \equiv \begin{cases} 0 & , u < 0 \\ 1 & , u > 0 \end{cases} . \qquad \text{(A3)}$$

To insure the consistency of $f_\alpha$ in the limit $\alpha \to 0$, we choose $h(0) = 1/2$.

Having set the initial conditions, we must now derive an equation for the circulation or vortex strength $\underset{\sim}{\kappa}(t)$ from Eq. (1) in the main text. We note that the vorticity is generated in the region containing the heated gas, denoted here by F, which corresponds to the flame. The region F and the associated residual vorticity then move with the fluid behind the incident shock after the shock has passed through the flame. Given a volume of fluid $\Omega(t)$ containing the region F, we have (Meyer, 1982)

$$\int_{\Omega(t)} \left( \frac{d\underset{\sim}{\xi}}{dt} + \underset{\sim}{\xi}\, \underset{\sim}{\nabla} \cdot \underset{\sim}{v} \right) dV = \frac{d}{dt} \int_{\Omega(t)} \underset{\sim}{\xi}\, dV. \qquad \text{(A4)}$$

In this paper, we are considering only variations in the x-y plane, so that $\xi_z \neq 0$, $\xi_x = \xi_y \equiv 0$ and $\underset{\sim}{\xi} \cdot \underset{\sim}{\nabla v} \equiv 0$. Since the integrands do not vary with z, Eqs. (1) and (A4) give us

$$\frac{d\kappa_z}{dt}(t) \equiv \frac{d}{dt} \int_{A(t)} \xi_z \, dA(t) = \int_{A(t)} [(\underset{\sim}{\nabla}\rho \times \underset{\sim}{\nabla}P)_z / \rho^2] \, dA(t). \qquad \text{(A5)}$$

To determine the vorticity generated by a shock passing through F, we need to integrate eq. (A5) over the interval $\tau$ during which the shock interacts with F. In the case which we are considering, F has a radius $S_o \sim$

2.5 cm. The interaction (shock transit) time will then be quite short compared to the time scales of flame propagation and vortex-induced rotational motion. The area A(t) containing F and nonzero vorticity will change due to the motion of the fluid behind the shock and the compression of fluid elements by the shock. For weak shocks these will also be small effects, and we will assume that $A(t) \approx A_0$, where $A_0$ is the area containing F prior to the arrival of the shock. In other words, we assume that the Jacobian matrix of the transformation from dA(t) to $dA_0$ is approximately the identity matrix. Thus we obtain

$$\kappa_z(t) \approx \int_{-\tau/2}^{t} dt' \int_{A_0} dx\, dy\, [(\nabla\rho \times \nabla P)_z / \rho^2]. \qquad (A6)$$

To compute $\kappa_z(t)$ for a single vortex in the upper half plane, we use

$$\kappa_z(t) \approx \int_{-\infty}^{t} dt \int_{-\infty}^{\infty} dx \int_{0}^{\infty} dy\, [(\nabla\rho \times \nabla P)_z / \rho^2]. \qquad (A7)$$

In Eq.(A7), we have extended the limits of the integrals to the entire half plane and $t \to -\infty$ for convenience in performing the theoretical calculations. This is reasonable as long the intensity of the interaction drops off rapidly as time decreases from $t = -\tau/2$.

We will compute the vortex strength in Eq.(A7) in the limit that the shock has infinitesimal thickness ($\alpha \to 0$). We assume for convenience that the density profile of the heated region is given by

$$\rho(\underset{\sim}{s}, t) = \rho_\infty \exp\,[-\, g(s/S_0,\, t)\; \ell n(\rho_\infty/\rho_0)], \tag{A8}$$

where $\underset{\sim}{s}$ is the displacement from the center of the region and $g(s/S_0,t)$ is a function defined so that $g(0,t) = 1$ and $\lim_{s\to\infty} g(s/S_0,t) = 0$. For brevity we will use $g(s) \equiv g(s/S_0,t)$ in subsequent equations. In the limit $\alpha \to 0$, the source term in Eq. (1) for $t < 0$ becomes

$$\frac{1}{\rho^2}\underset{\sim}{\nabla}\rho \times \underset{\sim}{\nabla}P = -\,\underset{\sim}{e}_z \sin\theta \frac{\partial g}{\partial s} \ln\left(\frac{\rho_\infty}{\rho_0}\right)\; \delta\left(\frac{s\cos\theta}{Wt} - 1\right) \times \tag{A9}$$

$$\times \left[\frac{-\, v_2 s\cos\theta}{Wt^2} + \frac{v_2^2\, h\left(\frac{s\cos\theta}{Wt} - 1\right)}{Wt}\right],$$

since the derivative $h'(u) = \delta(u)$. To derive Eq. (A9), we have computed $\underset{\sim}{\nabla}P$ from the equation of motion

$$\frac{d\underset{\sim}{v}}{dt} = -\,\frac{1}{\rho}\,\underset{\sim}{\nabla}P\ . \tag{A10}$$

In computing $\kappa$ from Eqs. (A7) and (4) (main text), we notice that the integral over the interval $(-\infty,0)$ for $t < 0$ is identical to that over the interval $(0,\infty)$ for $t > 0$, so that we need only double the result for either interval to determine the residual vortex strength. (In practice the time integral is negligible outside the interval $(-\tau/2,\ \tau/2)$, where $\tau$ is the time scale of the shock and flame interaction.)

Equation (A7) now gives us

$$\kappa \approx 2 \ln \left(\frac{\rho_\infty}{\rho_0}\right) \int_{-\infty}^{0} dt \int_{\pi/2}^{\pi} d\theta(-\sin\theta) \int_{0}^{\infty} ds\, s\left\{ \frac{\partial g}{\partial s}\, \delta\left(\frac{s\cos\theta}{Wt} - 1\right) \times \right. \tag{A11}$$

$$\left. \times \left[\frac{v_2^2 h\left(\frac{s\cos\theta}{Wt} - 1\right)}{Wt} - \frac{v_2 s\cos\theta}{Wt^2}\right]\right\} .$$

With a change of variables to $\beta = s\cos\theta/Wt - 1$, Eq. (A11) becomes

$$\kappa \approx 2 \ln \left(\frac{\rho_\infty}{\rho_0}\right) \int_{-\infty}^{0} dt \int_{\pi/2}^{\pi} d\theta(-\sin\theta) \left.\frac{\partial g}{\partial \beta}\right|_{\beta=0} \left[\frac{v_2^2 h(0)}{Wt} - \frac{v_2}{t}\right] \frac{Wt}{\cos\theta} . \tag{A12}$$

Application of the chain rule of differentiation results in

$$\left.\frac{\partial g}{\partial \beta}\right|_{\beta=0} = \frac{Wt}{\cos\theta} \left.\frac{\partial g}{\partial s}\right|_{s=Wt/\cos\theta} , \tag{A13}$$

which permits a change of variables to $\zeta = Wt/\cos\theta$. Equation (A12) is then

$$\kappa \approx 2 \ln \left(\frac{\rho_\infty}{\rho_0}\right) \int_{-\infty}^{0} dt\, Wt \left[\frac{v_2^2 h(0)}{Wt} - \frac{v_2}{t}\right] \int_{-Wt}^{\infty} d\zeta \frac{\partial g}{\partial \zeta}$$

$$= 2 \ln \left(\frac{\rho_\infty}{\rho_0}\right) v_2 [W - v_2/2] \int_{0}^{\infty} dt\, g(Wt). \tag{A14}$$

Because $W > v_2$ and $\rho_\infty > \rho_0$, we see that the direction of the vorticity in Eq. (A14) agrees with that in Figs. 1 and 5. We may define a form factor f by

$$f = \frac{2}{\tau} \int_{0}^{\infty} dt\, g(Wt), \tag{A15}$$

where $\tau \equiv 2\, S_0/W$, so that

$$\kappa \approx 2\, v_2\, (W - v_2/2) \left(\frac{\tau}{2}\right) \ell n \left(\frac{\rho_\infty}{\rho_0}\right) f$$

$$\approx 2\, v_2\, (1 - v_2/2W)\, S_0\, \ell n \left(\frac{\rho_\infty}{\rho_0}\right) f. \tag{A16}$$

Note that we have previously defined $g(s) \equiv g(s/S_0)$. For a Gaussian form,

$$g(s/S_0) = \exp\ (-\ s^2/S_0{}^2) \tag{A17}$$

we have $f = \sqrt{\pi}/2$, while for a square wave

$$g(s/S_0) = \begin{cases} 1 & s/S_0 < 1 \\ 0 & s/S_0 > 1 \end{cases}, \tag{A18}$$

$f = 1$. For the Bennett profile used in the simulation, Eq. (8), f will be less than $\sqrt{\pi}/2$ (Picone and Boris, 1983).

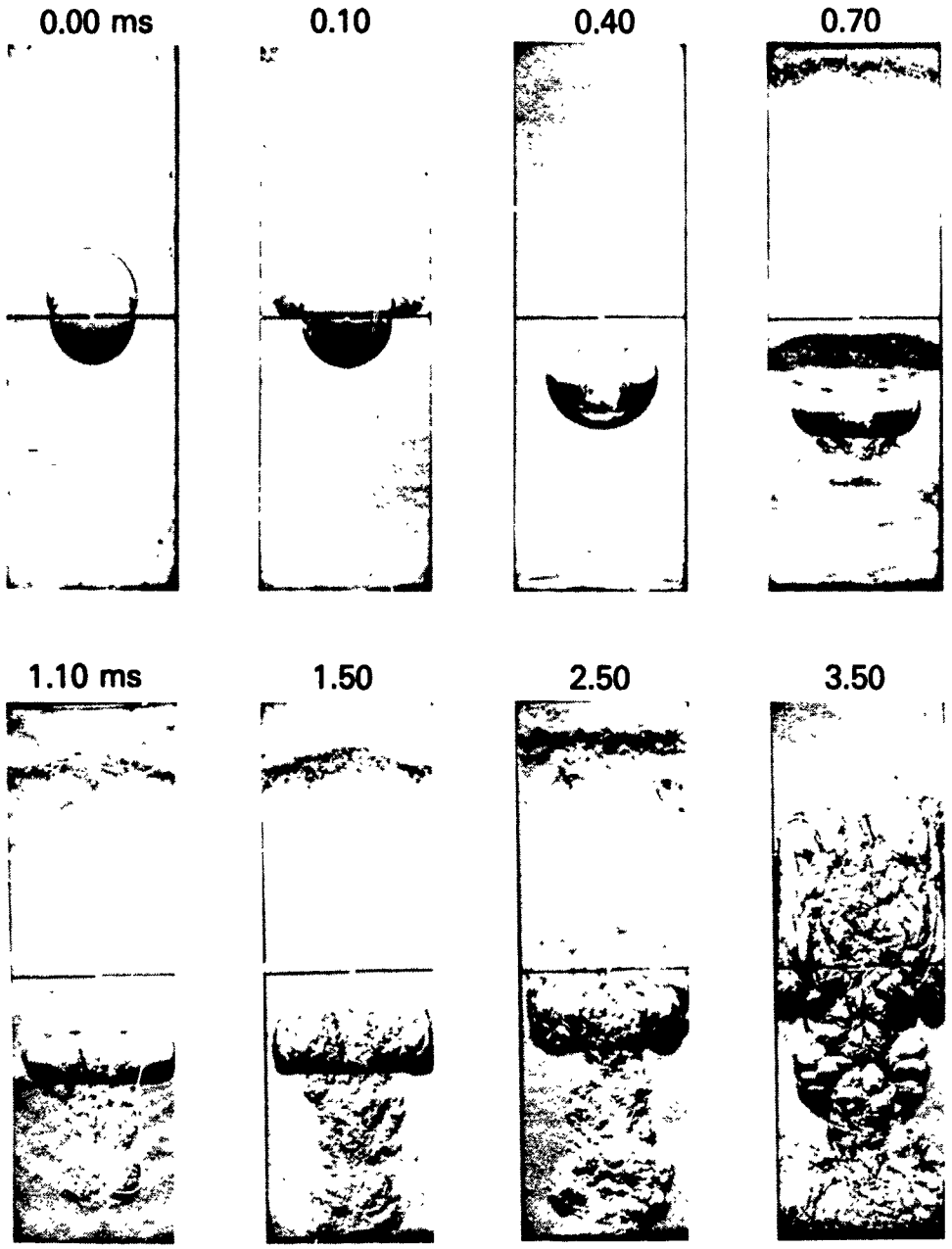


Fig. 1. "Interaction between a shock wave and a flame of initially roughly spherical shape. Pressure ratio of incident shock wave 1.3; stoichiometric n-butane-air mixture ignited at center of combustion chamber 8.70 ms before origin of time scale." (Rudinger, 1958 and Markstein, 1964) (Reprinted by permission of Pergamon Press, Inc.).

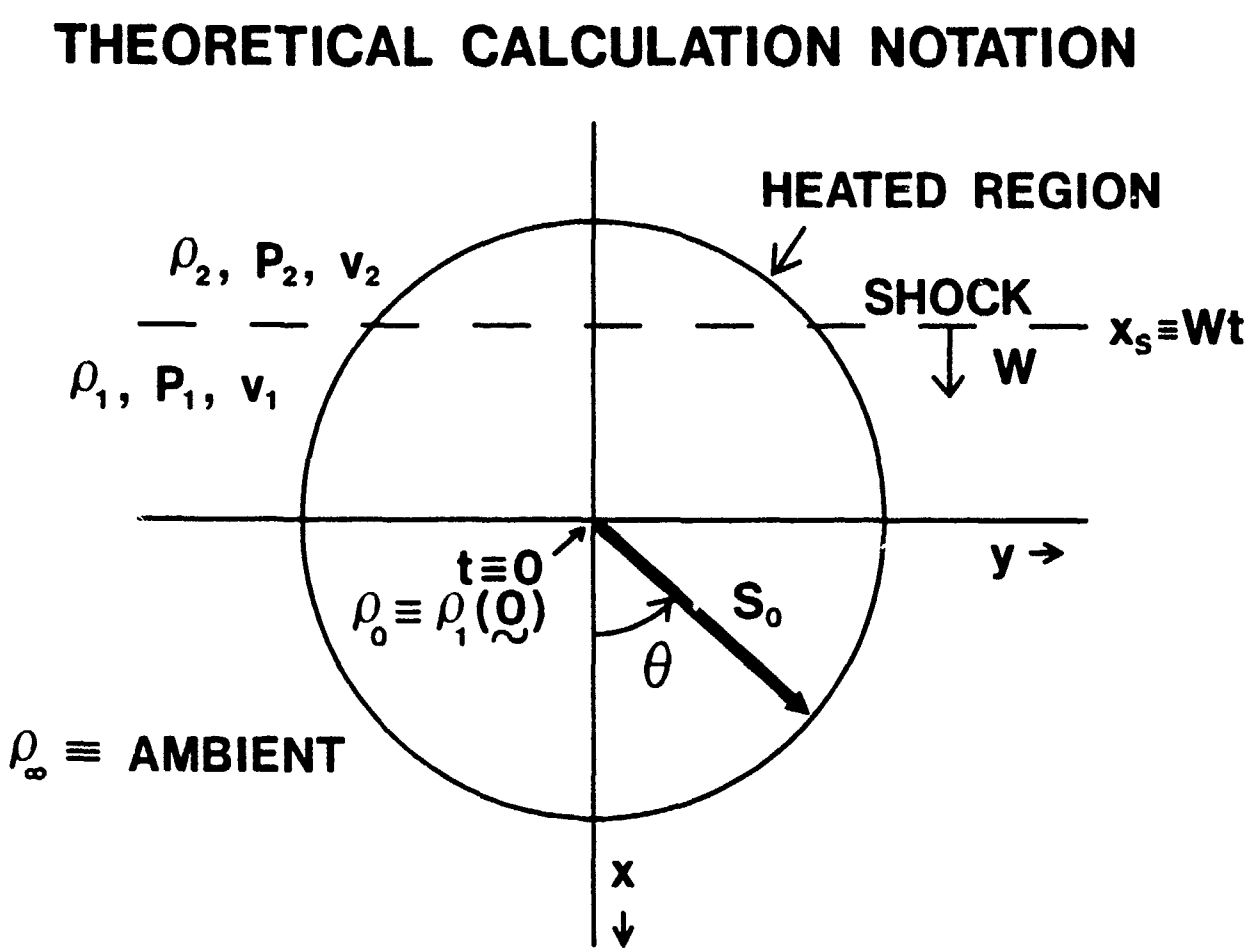


Fig. 2. Diagram defining terms for calculation of vorticity strength in the section on theory and in the appendix.

# NUMERICAL SIMULATION

$t_s = 9.4 \times 10^{-5} s$

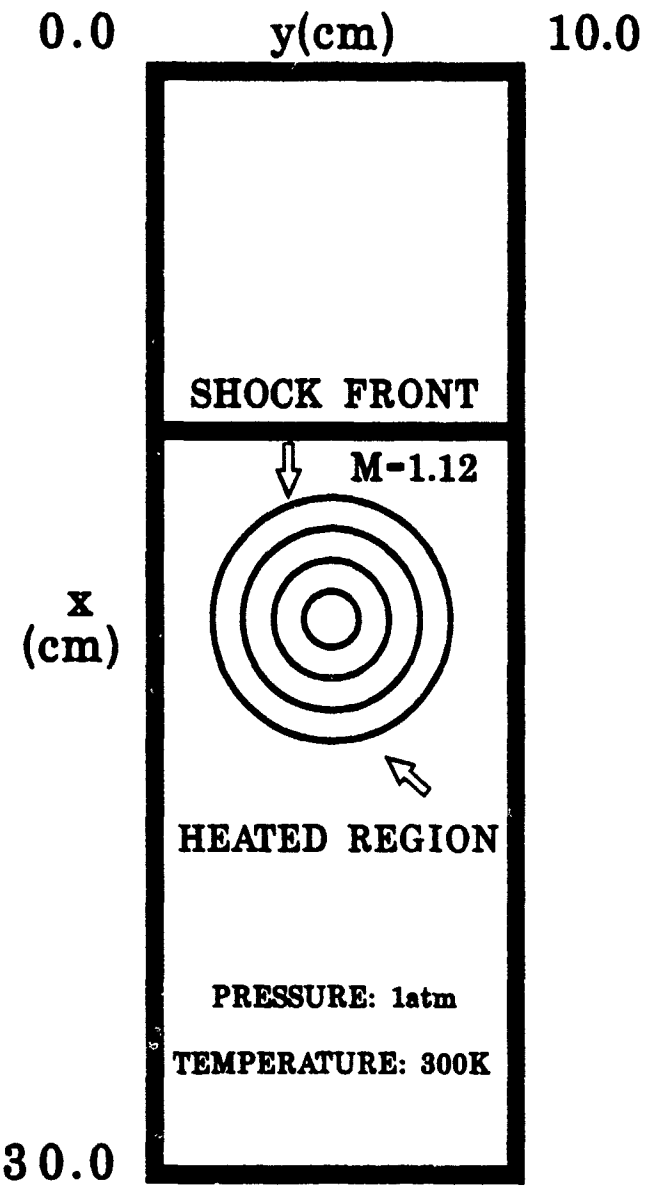


Fig. 3. Density contour diagram shortly after the simulation began. The dimensions of the chamber are similar to those in Fig. 1. Gas flows into the chamber from the top boundary.

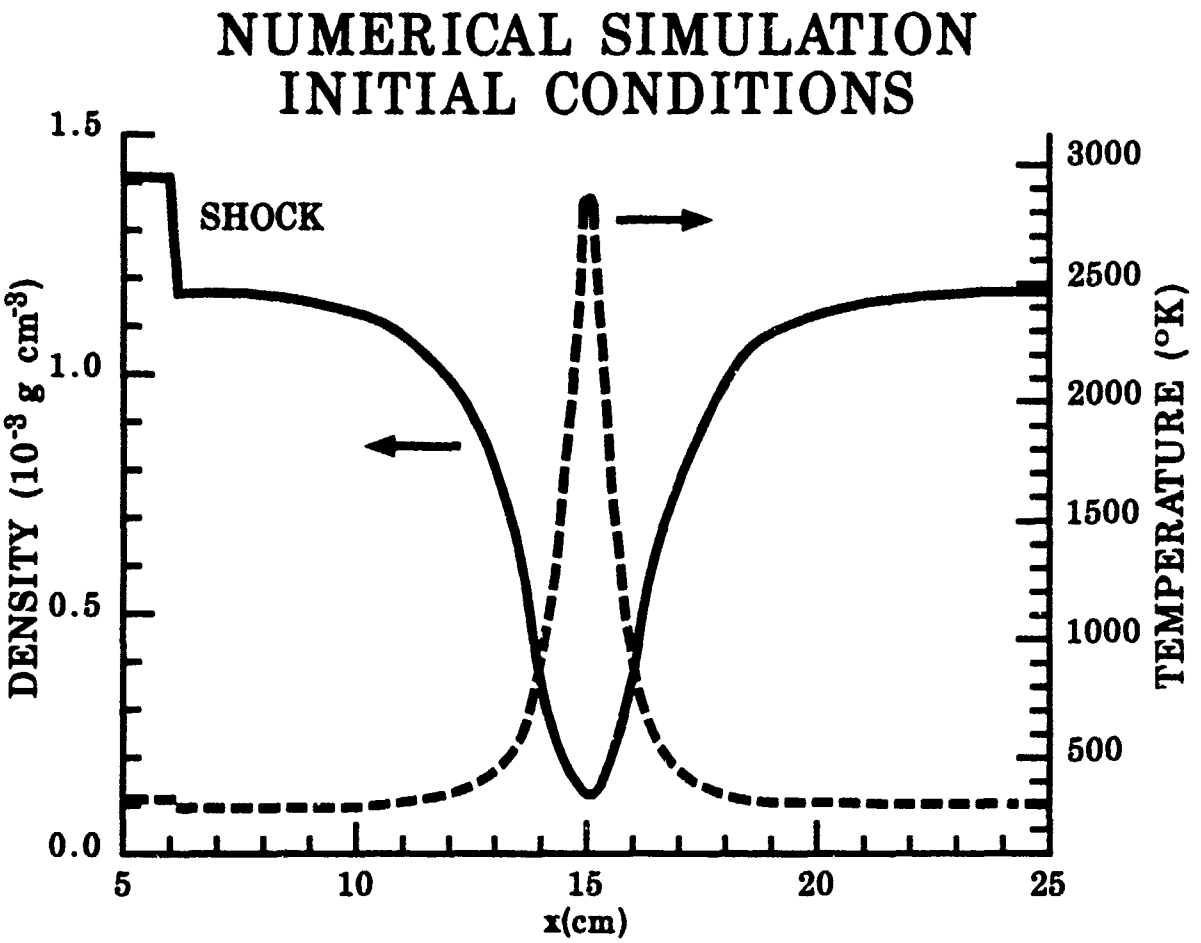


Fig. 4. The density and temperature distributions at simulation time $t_s$=0 show the shock at the left and the heated region in the center of the grid.

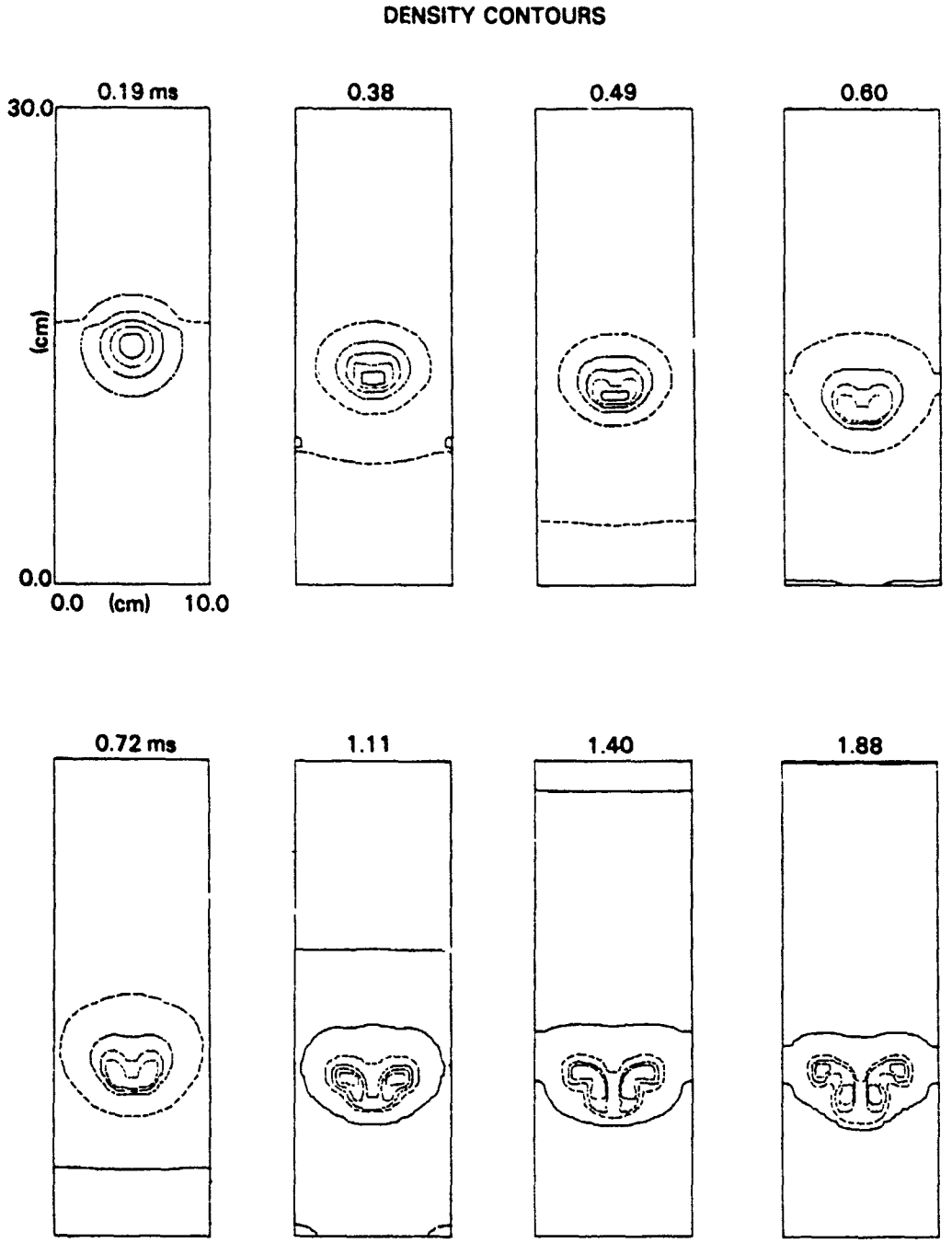


Fig. 5. Density contour diagrams at given times $t_s$. In the first three frames the six contours range from $3 \times 10^{-4}$ to $1.5 \times 10^{-3}$ g/cm$^3$ in equal increments while in the last five, the contours range from $3 \times 10^{-4}$ to $1.6 \times 10^{-3}$ g/cm$^3$. Notice the Mach structure at the channel boundary at $t_s$=384 μs.

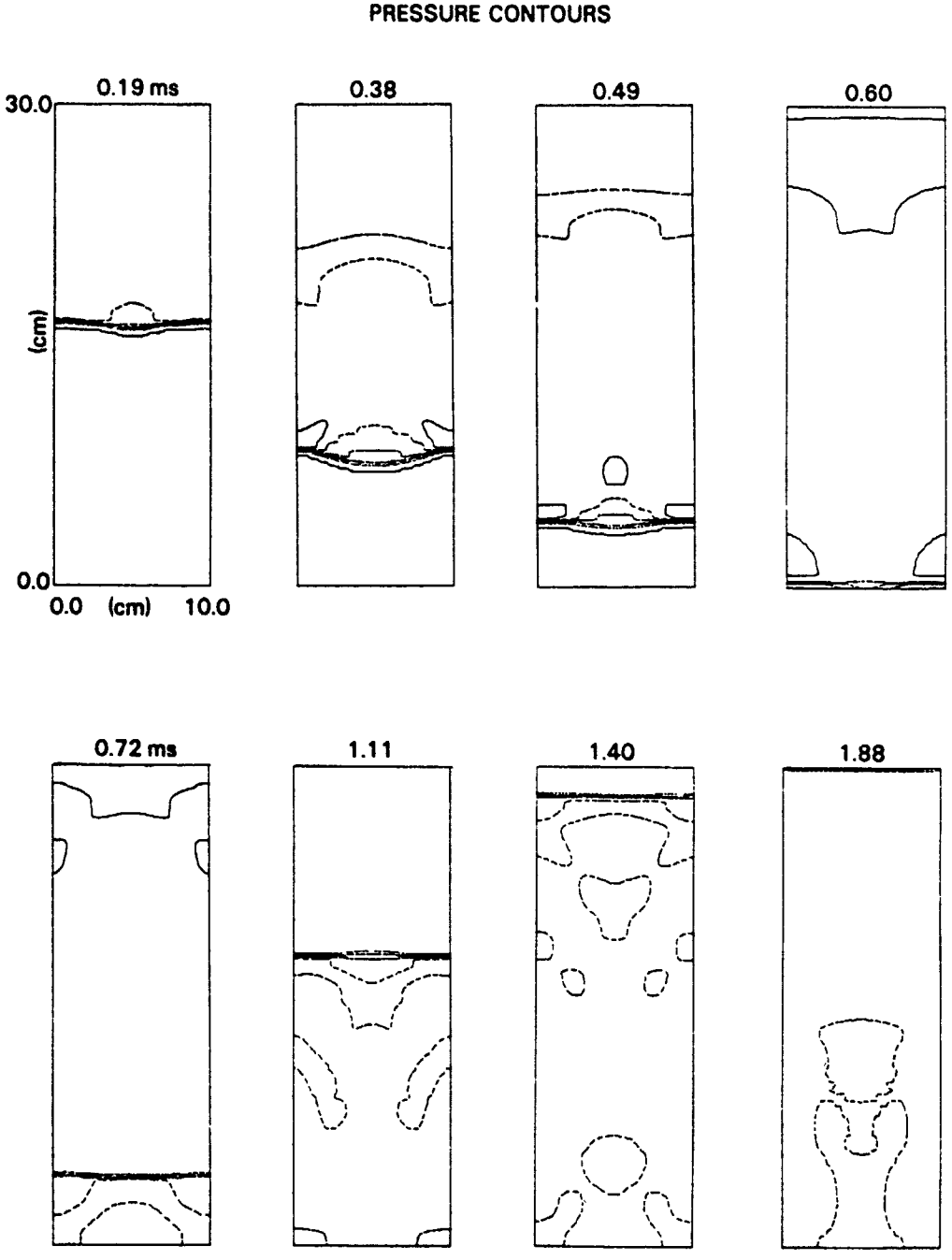


Fig. 6. Pressure contour diagrams at given times $t_s$. In the first three frames the contours range from $1.02 \times 10^6$ to $1.35 \times 10^6$ dyne/cm$^2$ in equal increments. In the last five the range is $1.3 \times 10^6$ to $1.8 \times 10^6$ dyne/cm$^2$. Again notice the Mach structure prior to reflection at the bottom boundary.

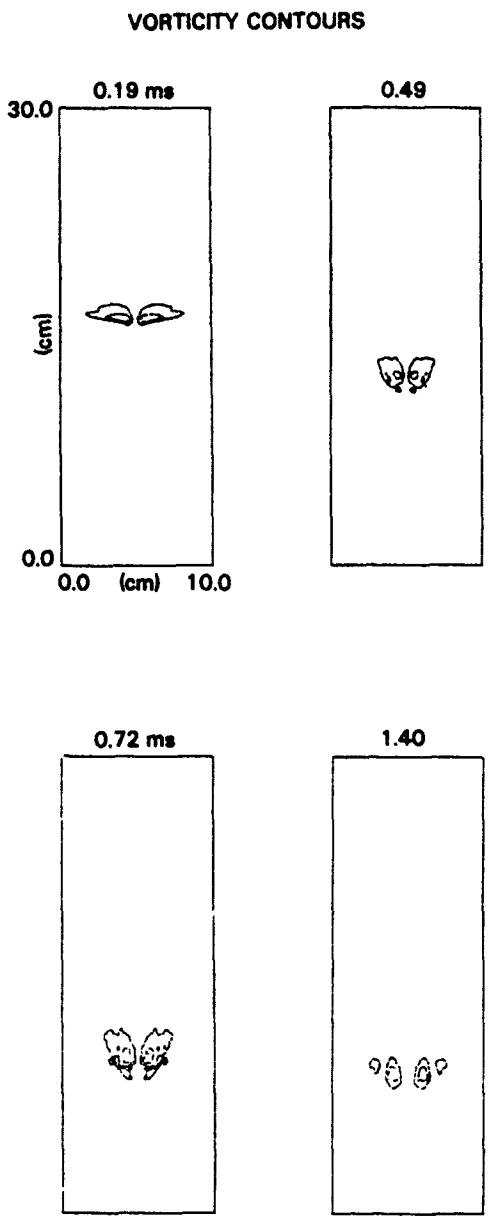


Fig. 7. Vorticity contour diagrams at given times $t_s$. The ranges of vorticity values (respectively from earliest to latest times) are $\pm 3 \times 10^3$ $s^{-1}$, $\pm 1.5 \times 10^4$ $s^{-1}$, $\pm 1.1 \times 10^4 s^{-1}$, and $\pm 1.8 \times 10^4 s^{-1}$. The number of vortex centers and the peak vorticity increase after the reflected shock passes through the heated region (last frame), as anticipated. Corresponding vortices in each frame are oppositely directed and oriented to pull fluid from top to bottom.

## REFERENCES


Book, D.L., Boris, J.P.; Kuhl, A.L.; Oran, E.S.; Picone, J.M.; and Zalesak, S. T. (1981) Simulation of complex shock reflections from wedges in inert and reactive gaseous mixtures. Proceedings of the Seventh International Conference on Numerical Methods in Fluid Dynamics, Springer-Verlag, New York, pp. 84-90.

Boris, J.P. and Book, D.L. (1976) Solution of continuity equations by the method of flux-corrected transport. Methods in Computational Physics, Vol.16, Academic Press, New York, pp. 85-129.

Chu, B.-T. and Kovásznay, L.S.G. (1957) Non-linear interactions in a viscous heat-conducting compressible gas. J. Fluid Mech. 3, 494-514.

Markstein, G.H. (1964) Experimental studies of flame-front instability. Nonsteady Flame Propagation, AGARDograph No. 75, Pergamon Press, Oxford, pp. 75-100.

Meyer. R.E. (1982) Introduction to Mathematical Fluid Dynamics, Dover Publications, Inc., New York, Chapt.1.

Oran, E.S.; Young, T.R.; Boris, J.P.; Picone, J.M.; and Edwards, D.H. (1983) A study of detonation structure: the formation of unreacted gas pockets. Proceedings of the Nineteenth Symposium (International) on Combustion, The Combustion Institute, Pittsburgh, PA, pp. 573-582.

Picone, J.M. and Boris, J.P. (1983) Vorticity generation by asymmetric energy deposition in a gaseous medium. Phys. Fluids, 26, 365-382.

Rudinger, G. (1958) Shock wave and flame interactions. Combustion and Propulsion, Third AGARD Colloquium, Pergamon Press, New York, pp. 153-182.